Nanoscale Res Lett (2007) 2:569–575
DOI 10.1007/s11671-007-9101-5

NANO EXPRESS

Fine Splitting of Electron States in Silicon Nanocrystal with a Hydrogen-like Shallow Donor

Vladimir A. Belyakov · Vladimir A. Burdov

Received: 7 July 2007 / Accepted: 16 October 2007 / Published online: 2 November 2007

Abstract Electron structure of a silicon quantum dot doped with a shallow hydrogen-like donor has been calculated for the electron states above the optical gap. Within the framework of the envelope-function approach we have calculated the fine splitting of the ground sixfold degenerate electron state as a function of the donor position inside the quantum dot. Also, dependence of the wave functions and energies on the dot size was obtained.

Keywords Silicon nanocrystal · Donor · Energy spectrum · Fine splitting

Introduction

Introduction of shallow impurities into silicon quantum dots is considered [1–5] as an efficient way to modify optical properties of the dots. In connection to this, calculations of electronic structure [6–11] and dielectric function [12–18] of silicon nanocrystals doped with V-group shallow donors have been carried out earlier. The microscopic first-principles study of charge distribution and electrostatic fields in bulk silicon [19–21] and silicon crystallites [16–18] in the presence of V-group donors have shown existence of short-range and long-range components of the electron–ion Coulomb interaction in the system. The short-range potential differs from zero only in a nearest vicinity (about Bohr radius) of the donor nucleus. This extra potential, frequently named a "central-cell correction", leads to so-called valley–orbit interaction [22, 23]. In turn, the valley–orbit interaction causes the splitting of the electron ground state that is sixfold degenerate if the spin variables have not been taken into account. The degeneracy order exactly coincides with the number of valleys in a conduction band of bulk silicon. The long-range component represents standard ε-times weakened Coulomb attraction between the donor ion and electron.

Quantum confinement in nanocrystals considerably strengthens the valley–orbit interaction and level splitting [8–11] relative to the bulk systems [24]. Provided that the valley–orbit interaction is strong, the sixfold degenerate lowest energy level splits into three (if the donor occupies the dot center) or six (if the donor position is arbitrary) levels. In case of symmetric central-located donor position in the nanocrystal the ground state splits into a singlet, doublet, and triplet [8, 10, 11], as it takes place in the bulk silicon [22, 23], the singlet level being strongly split off from the doublet and triplet levels and always turns out to be the lowest one.

However, not all the donors manifest strong valley–orbit coupling. For example lithium, being interstitial donor of the first group, has the splitting of about 1–2 meV [24] which is one-two order less than that for V-group donors such as P, As, Sb, and Bi. It is, therefore, logical to assume also for quantum dots (without resorting to calculations), that the valley–orbit splitting and central-cell effect for Li will be weakened compared to the V-group donors by the same order of magnitude. As was shown for 2–5 nm nanocrystals [10, 11], maximal values of the splitting for the V-group donors are of the order of several tenths of eV. As a consequence, the valley–orbit splitting for Li in the dot does not exceed, presumably, 10 meV. At the same time, as will be shown below, the splitting caused by the

V. A. Belyakov (✉) · V. A. Burdov
Department of Theoretical Physics, University of Nizhniy Novgorod, Nizhniy Novgorod 603950, Russia
e-mail: vab3691@yahoo.com

long-range hydrogenic potential turns out to be considerably greater (about 100 meV). This indicates a key role of the hydrogenic potential compared to the central-cell one for Li. On this reason, the hydrogenlike model may be applied to a lithium donor in a silicon nanocrystal. Therefore, when dealing with Li-doped dots, we shall neglect the short-range central-cell field and, consequently, the valley–orbit splitting.

In turn, for V-group donors in quantum dots, a contribution of the long-range field to the energy splitting is 3–5 times less than that of the short-range field. In particular, in the works of the authors [10, 11] electronic structure of silicon crystallites doped with V-group donors has been already calculated in the presence of both short- and long-range Coulomb interactions. Note, however, that the results of Refs [10, 11] may not be automatically extended to Li-doped nanocrystals by zero setting the terms caused by the short-range field. For V-group donors the central-cell potential, being stronger than the hydrogenic one, imposes certain symmetry to the Bloch states. The latter are described by the functions possessing A_1, E, or T_2 symmetry. Existence of the hydrogen-like potential leads to some insignificant corrections only. In case of a lithium donor, the situation is opposite. Precisely the hydrogen-like potential is a dominant factor, while the valley–orbit interaction is negligibly small. As a result, we have to use different approaches to solve the problem. Consequently, the solutions obtained in these two cases are appreciably different.

In the present article we find the energies and wave functions of the ground and several excited electronic states of silicon quantum dot with a lithium donor that may be treated as a shallow hydrogenic one. We shall also discuss an effect of degeneracy removal caused by the presence of a hydrogenlike center in an arbitrary place inside the dot, and calculate the splitting of the lowest energy level being sixfold degenerate initially.

For this purpose we employ envelope-function approximation. Of course, an applicability of the $\mathbf{k}\cdot\mathbf{p}$ method to quantum dots is justified when the dot size considerably exceeds the size of the unit cell. The latter approximately coincides with the distance between adjacent atoms in silicon lattice (2.35 Å). We suppose this requirement to be fulfilled for 2–5 nm nanocrystals. In this case, keeping ourselves within the framework of a macroscopic picture, one can use bulk static dielectric constants ε_s and ε_d for materials inside and outside the dot, respectively. As a result, the standard Coulomb potential is modified due to appearance of polarization charges at the nanocrystal boundary [13, 14]. Existence of an excess positive charge near the dot boundary has been directly confirmed by the microscopic first-principles calculations of Delerue et al. [16] and Trani et al. [18].

The Model and Basic Equations of the Problem

Let us consider a silicon quantum dot of radius R, embedded into a wide-band matrix such as SiO_2. The potential barriers for electrons caused by the band discontinuity at the dot boundary are of the order of several eV. Since the typical energies we shall further consider do not exceed a few tenths of eV, the barriers may be treated as infinitely high.

Within the frames of macroscopic treatment the total electron potential energy $U(\mathbf{r})$ consists of three parts:

$$U(\mathbf{r},\mathbf{h}) = U_0(r) + V_{sp}(r) + V_{ie}(\mathbf{r},\mathbf{h}). \tag{1}$$

Here $\mathbf{r}$ and $\mathbf{h}$ are the position-vectors of the electron and impurity ion, respectively. $U_0(r)$ is the potential of an infinitely deep well that is assumed to be zero inside, and infinity outside, the dot. The second part $V_{sp}(r)$ describes an interaction between the electron and its own image arising due to the charge polarization on the boundary between silicon and silicon dioxide. Since the electron interacts with its own image, $V_{sp}(r)$ is frequently referred to as a self-polarization term. It can be represented in the form, see, e.g., Eqs (3.24), (3.26) in Ref. [25]:

$$V_{sp}(r) = \frac{e^2(\varepsilon_s-\varepsilon_d)}{2\varepsilon_s R}\sum_{l=0}^{\infty}\frac{l+1}{l\varepsilon_s+(l+1)\varepsilon_d}\frac{r^{2l}}{R^{2l}}. \tag{2}$$

At last, the third term $V_{ie}(\mathbf{r},\mathbf{h})$, introduced in the Eq. 1, represents an electron–ion interaction. It has the form [25]:

$$V_{ie}(\mathbf{r},\mathbf{h}) = -\frac{e^2}{\varepsilon_s|\mathbf{r}-\mathbf{h}|} - \frac{e^2(\varepsilon_s-\varepsilon_d)}{\varepsilon_s R} \times \sum_{l=0}^{\infty}\frac{h^l r^l}{R^{2l}}\frac{l+1}{l\varepsilon_s+(l+1)\varepsilon_d}P_l(\cos\theta), \tag{3}$$

where θ is the angle between $\mathbf{h}$ and $\mathbf{r}$. The first term in the expression (3) corresponds to the direct Coulomb attraction between the donor and electron, while the second term, represented by the sum over l, describes an interaction between the ion image and electron. This term disappears when ε_s and ε_d become equal.

Notice that $U_0(r)$ and $V_{sp}(r)$ are isotropic functions independent of the electron position-vector direction. On the contrary, the electron–ion interaction strongly depends on the positional relationship of the ion and electron. As a consequence, the direction of $\mathbf{r}$ influences the magnitude of V_{ie}.

In order to determine the electron states we have to solve the single-particle Schrödinger-like equation for the envelope functions $F_j(\mathbf{r})$ and the electron energy E:

$$\left(H_{ij}+U(\mathbf{r},\mathbf{h})\delta_{ij}\right)F_j(\mathbf{r}) = EF_i(\mathbf{r}). \tag{4}$$

Here, H_{ij} is the matrix $\mathbf{k}\cdot\mathbf{p}$ Hamiltonian operator for bulk Si, and the Einstein convention has been applied for

summing over j. It is well known that energy minima in the conduction band of silicon are located nearby X-points symmetrically relative to the boundary of the Brillouin zone. At the X-point energy branches intersect, which leads to the double degeneracy. Since there are three physically nonequivalent X-points in the conduction band, the spectrum is sixfold degenerate on the whole (without spin) as was already mentioned above.

Frequently, when analyzing electron phenomena in silicon, the model of parabolic energy band with longitudinal $m_l = 0.92m_0$ and transverse $m_t = 0.19m_0$ effective masses is used. However, such a representation is correct for electron energies obeying the inequality $|E - E_\Delta| \ll |E_X - E_\Delta|$, where E_X and E_Δ are, respectively, the energies of the X-point and the point of the energy minimum located at the Δ-direction. It is not so in our case. Due to the strong quantum confinement, typical electron energies are of the order of, or even greater than [26–28], the energy difference $E_X - E_\Delta = 0.115$ eV [29]. Therefore, interplay between the two crossing branches must be taken into account. This requires more accurate consideration of the electronic dispersion low, outgoing the frames of parabolic approximation.

This has been done by Kopylov [29] for bulk semiconductors. We use here for the quantum dot the Kopylov's $\mathbf{k}\cdot\mathbf{p}$ Hamiltonian operator written in a basis of two Bloch states $\{|X\rangle, |X'\rangle\}$, $\{|Y\rangle, |Y'\rangle\}$, or $\{|Z\rangle, |Z'\rangle\}$ for each of three nonequivalent X-points in the Brillouin zone. All the Bloch functions belong to the spinless irreducible representation X_1 of an X-point. Let us consider, for definiteness, the X-point along the direction (0, 0, 1). Then the wave function is expanded as $\Psi = F(\mathbf{r})|Z\rangle + F'(\mathbf{r})|Z'\rangle$, where $F(\mathbf{r})$ and $F'(\mathbf{r})$ are slow envelope functions being the expansion coefficients in the Bloch-state basis $\{|Z\rangle, |Z'\rangle\}$. The bulk $\mathbf{k}\cdot\mathbf{p}$ Hamiltonian operator may be written as the sum of isotropic and anisotropic parts: $H_{ij} = H_{ij}^{(0)} + H_{ij}^{(1)}$, where the former is represented by $H_{ij}^{(0)} = (\mathbf{p}^2/2m_e)\delta_{ij}$ with the effective electron mass $m_e = 3m_l\ m_t\ /(2m_l + m_t)$. Such the explicit form of $H_{ij}^{(0)}$ is obtained as the average of H_{ij} over angles in the $\mathbf{p}$-space. The anisotropic part is defined with the following expression:

$$H_{ij}^{(1)} = \begin{pmatrix} \left(\frac{1}{m_t} - \frac{1}{m_l}\right)\frac{\mathbf{p}^2 - 3p_z^2}{6} & \left(\frac{1}{m_t} - \frac{1}{m_0}\right)p_x p_y + i\frac{p_0 p_z}{m_l} \\ \left(\frac{1}{m_t} - \frac{1}{m_0}\right)p_x p_y - i\frac{p_0 p_z}{m_l} & \left(\frac{1}{m_t} - \frac{1}{m_l}\right)\frac{\mathbf{p}^2 - 3p_z^2}{6} \end{pmatrix}. \tag{5}$$

Here $p_0 = 0.144(2\pi\hbar/a_0)$ is the distance from the X-point to any of the two nearest energy minima in the $\mathbf{p}$-space, $a_0 = 0.543$ nm stands for the lattice constant of silicon. The quasimomentum $\mathbf{p}$ and the energy E have the origin at the X-point.

Equation 4 for an undoped nanocrystal has been already solved earlier [26]. In the following we shall employ, in fact, the solutions obtained in Ref. [26] as the zeroth approximation of the problem with a doped dot.

Because of the isotropic and diagonal form of the operator $H_{ij}^{(0)} + U_0(r)\delta_{ij}$, it is possible to classify its eigenstates similarly to atomic systems as the states of s-, p-, d-type, etc. Accordingly, one may expand the envelope functions over these eigenstates as:

$$F_j(\mathbf{r}) = \sum_\alpha C_{j\alpha}|\alpha\rangle, \tag{6}$$

where $|\alpha\rangle$ denote the s-, p-, d-,... states, and $C_{j\alpha}$ are the expansion coefficients. As was shown in Ref. [26], in order to find energies and wave functions of a few lower states with an accuracy of about several percent, it is sufficient to keep in the expansion (6) only s- and p-states, so that $|\alpha\rangle$ becomes equal to $|s\rangle$ or $|p_a\rangle$ with $a = x, y, z$.

Substitution of the expansion (6) into Eq. 4 yields algebraic equations for $C_{j\alpha}$:

$$\begin{aligned} (E - E_s)C_{is} =& \langle s|H_{ij}^{(1)} + V(\mathbf{r},\mathbf{h})|s\rangle C_{js} \\ &+ \langle s|H_{ij}^{(1)} + V(\mathbf{r},\mathbf{h})|p_a\rangle C_{ja}, \\ (E - E_p)C_{ia} =& \langle p_a|H_{ij}^{(1)} + V(\mathbf{r},\mathbf{h})|s\rangle C_{js} + \langle p_a|H_{ij}^{(1)} \\ &+ V(\mathbf{r},\mathbf{h})|p_b\rangle C_{jb}. \end{aligned} \tag{7}$$

Here $E_s = \hbar^2\pi^2/2m_eR^2$ and $E_p = \hbar^2\mu^2/2m_eR^2$ are the energies of the s- and p-states, $\mu = 4.4934$ is the first root of the spherical Bessel function $j_1(x)$. Explicit form of the matrix elements of the operators $H_{ij}^{(1)}$ and $V(\mathbf{r},\mathbf{h})$ can be found, e.g., in Ref. [10]. The energy E_s is doubly degenerate while the energy E_p is the sixfold level. Thus, solving Eq. 7 we should obtain, in general case, eight electron states.

Within the restricted basis of s- and p-type envelope states, which is used here, one can solve Eq. 7 analytically [26] if neglect $s-p_a$ Coulomb matrix elements $V_a(\mathbf{h}) \equiv \langle s|V(\mathbf{r},\mathbf{h})|p_a\rangle$ and anisotropic components of p_a-p_b type $V_{ab}(\mathbf{h}) \equiv \langle p_a|V(\mathbf{r},\mathbf{h})|p_b\rangle$ both for $a = b$ and $a \neq b$. Notice that the diagonal p_a-p_a Coulomb matrix elements consist of two parts [10]: isotropic $V_{pp}(h)$, and anisotropic $V_{aa}(\mathbf{h}) \sim h^2 - 3h_a^2$. As our numerical estimations show, the latter is much less than the former. For comparison we have plotted in Fig. 1 for 3 nm quantum dot both the anisotropic Coulomb matrix elements $V_z(\mathbf{h}), V_{xy}(\mathbf{h}), V_{zz}(\mathbf{h})$ and isotropic ones $V_{ss}(h) \equiv \langle s|V(\mathbf{r},\mathbf{h})|s\rangle$, $V_{pp}(h)$ versus h, in case the anisotropic matrix elements have their highest possible values. For instance, V_z and V_{zz} achieve their maximum when $h_x = h_y = 0$. On the contrary, V_{xy} has the greatest value for $h_z = 0$, $h_x = h_y$. As is seen in the figure, the anisotropic elements V_{xy} and V_{zz} are small compared to V_z. In turn, V_z is less than the diagonal isotropic matrix elements V_{ss} and V_{pp}. At last, all the Coulomb matrix

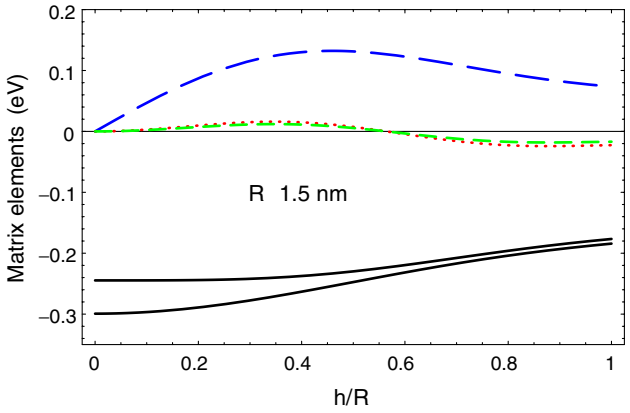

Fig. 1 Coulomb matrix elements versus dimensionless donor displacement from the dot center. Lower solid line—V_{ss}; Upper solid line—V_{pp}; Long-dashed line—V_z for $h_x = h_y = 0$; Short-dashed line—V_{zz} for $h_x = h_y = 0$; Dotted line—V_{xy} for $h_x = h_y$, $h_z = 0$

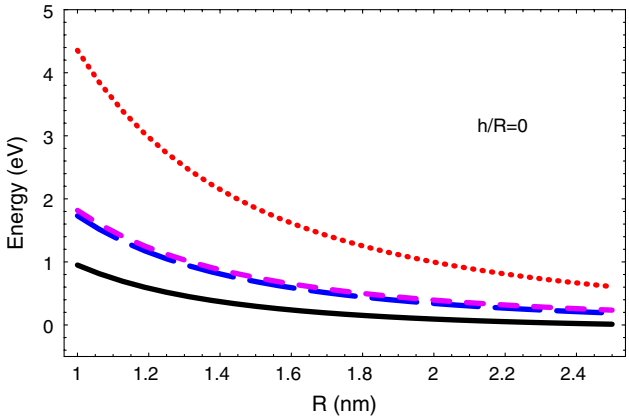

Fig. 2 Energies of the "isotropic" model ($V_a = 0$ in Eq. 7) as functions of the dot radius. From top to bottom: E_{3e}—dots; E_{2e}—short dash; E_{1e}—long dash; E_{0e}—solid line. All the energies are counted from the X-point energy

elements are substantially smaller than the difference $E_p - E_s$.

Results and Discussion

Solution of the simplified Eq. 7 for $V(\mathbf{r}, \mathbf{h}) \equiv 0$ has been obtained in Ref. [26]. There was shown that the twofold (s-type) and sixfold (p-type) levels split into four doubly degenerate levels due to the band anisotropy leading to the $s-p_z$ and p_x-p_y hybridization of the envelope states. The s−s and p−p diagonal Coulomb matrix elements in Eq. 7 contribute only to the shift of the unperturbed energy values: $E_s(h) = E_s + V_{ss}(h)$, $E_p(h) = E_p + V_{pp}(h)$. As a result, the twofold energies are written in the form:

$$
\begin{aligned}
E_{0e} &= \frac{E_s(h) + E_p(h) - 2H_{pp}}{2} \\
&\quad - \sqrt{\left(\frac{E_p(h) - E_s(h) - 2H_{pp}}{2}\right)^2 + H_{sp}^2}, \\
E_{1e} &= E_p(h) + H_{pp} - H_{xy}, \\
E_{2e} &= \frac{E_s(h) + E_p(h) - 2H_{pp}}{2} \\
&\quad + \sqrt{\left(\frac{E_p(h) - E_s(h) - 2H_{pp}}{2}\right)^2 + H_{sp}^2}, \\
E_{3e} &= E_p(h) + H_{pp} + H_{xy},
\end{aligned}
\tag{8}
$$

where the matrix elements of the band anisotropy $H_{sp} = 2\pi\hbar\mu p_0/\left[\sqrt{3}m_l R(\mu^2 - \pi^2)\right]$, $H_{pp} = \hbar^2\mu^2(m_l - m_t)/15m_t m_l R^2$, and $H_{xy} = \hbar^2\mu^2(m_0 - m_t)/5m_t m_0 R^2$ have been introduced.

The energy E_{3e} of the third excited doublet turns out to be strongly split off from the lower energies as is shown in Fig. 2. In the following we do not take this level into account because the two-level approximation, accepted in Eq. 7, is explicitly insufficient to describe correctly the upper electron states and their energies. The energies of the three lower levels E_{0e}, E_{1e}, and E_{2e} are also presented in Fig. 2 as functions of the dot radius R. One can see that, the level splitting due to the band anisotropy is great enough. The energy of the splitting turns out to be of the same order as the unperturbed energies E_s and E_p. However, in spite of such the strong splitting, the double degeneracy of all the levels is conserved. In order to lift it, the symmetry of the system must be violated. To this goal, one needs to introduce nonzero matrix elements $V_a(\mathbf{h})$ in Eq. 7, which reflect an asymmetry of the donor position inside the nanocrystal. At the same time, one may neglect, apparently, the terms $V_{ab}(\mathbf{h})$ and $V_{aa}(\mathbf{h})$ in Eq. 7 because of their small magnitudes, see Fig. 1.

The presence of nonzero $V_a(\mathbf{h})$ hampers solving Eq. 7. However, relative smallness of the off-diagonal Coulomb interaction with respect to the energies E_{je} allows one to apply a perturbation theory. It is important to emphasize that only the off-diagonal matrix elements $V_a(\mathbf{h})$ are treated as perturbation in this case, but not the Coulomb interaction $V(\mathbf{r}, \mathbf{h})$ on the whole.

An introduction of an asymmetry in the system leads to the total splitting of the energy levels. In particular, the lowest level splits into two energies $E_z^{(\pm)}$ equal to $E_{0e} - S_z \pm W_z$. Generally speaking, it is now possible to combine the results for all the three X-points and write down the energies of all the six lowest levels originated from the energy E_{0e} in the following form:

$$
E_a^{(\pm)} = E_{0e} - S_a \pm W_a. \tag{9}
$$

Here

$$S_a = \frac{V_a^2(\mathbf{h})}{E_{2e} - E_{0e}} + \frac{\left(V_b^2(\mathbf{h}) + V_c^2(\mathbf{h})\right)\cos^2\lambda}{2(E_{1e} - E_{0e})} \tag{10}$$

is the second-order shift of the energy E_{0e}, and the term W_a, defining the splitting, is

$$W_a = \frac{V_b(\mathbf{h})V_c(\mathbf{h})\cos^2\lambda}{E_{1e} - E_{0e}}. \tag{11}$$

This term leads to symmetric splitting of the energy $E_{0e} - S_a$ into two levels. Indices a, b, c enumerate the spatial axes. In Eqs. 10, 11 they do not coincide with each other. The notation "$E_a^{(\pm)}$" implies the solution obtained for the X-point located at a-direction in the $\mathbf{k}$-space. At last, the angle λ is defined by the following relationships:

$$\begin{aligned}\cos 2\lambda &= \frac{E_p(h) - E_s(h) - 2H_{pp}}{\sqrt{\left(E_p(h) - E_s(h) - 2H_{pp}\right)^2 + 4H_{sp}^2}},\\ \sin 2\lambda &= \frac{2H_{sp}}{\sqrt{\left(E_p(h) - E_s(h) - 2H_{pp}\right)^2 + 4H_{sp}^2}}.\end{aligned} \tag{12}$$

Notice that the level splitting appears only in the second order in $V_a(\mathbf{h})$. Contrary to this, wave functions, corresponding to the energies $E_a^{(\pm)}$, have the first-order corrections in $V_a(\mathbf{h})$:

$$\begin{aligned}\Psi_a^{(\pm)} = {} & \cos\lambda \frac{|A\rangle \pm |A'\rangle}{\sqrt{2}}|s\rangle \mp \sin\lambda \frac{|A\rangle \mp |A'\rangle}{\sqrt{2}}|p_a\rangle\\ & - \frac{V_a(\mathbf{h})\sec\lambda}{E_{2e} - E_{0e}} \frac{|A\rangle \pm |A'\rangle}{\sqrt{2}}|p_a\rangle\\ & - \frac{\cos\lambda}{E_{1e} - E_{0e}} \frac{V_b(\mathbf{h}) \mp V_c(\mathbf{h})}{\sqrt{2}} \frac{|A\rangle \pm |A'\rangle}{\sqrt{2}} \frac{|p_b\rangle \mp |p_c\rangle}{\sqrt{2}}.\end{aligned} \tag{13}$$

Here, the capital letter A runs the values X, Y, Z and defines the Bloch state of an X-point. It is important to note that index A describes the Bloch function of the X-point situated precisely at the k_a-axis in the Brillouin zone, i.e., in a certain sense, the small and big indices coincide.

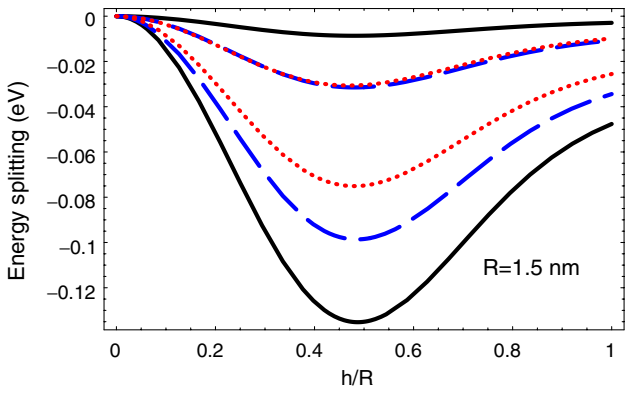

Fig. 3 Fine structure of the energy spectrum at $h_x/h = 0.8$, $h_y/h = 0.5$, $h_z/h = 0.33$ with respect to the unperturbed sixfold degenerate energy level E_{0e}. Solid lines—$E_z^{(\pm)}$; Dashed lines—$E_y^{(\pm)}$; Dots—$E_x^{(\pm)}$; The "+"-sign corresponds to the upper curves

The ground-level splitting is shown in Fig. 3. If the impurity position-vector $\mathbf{h}$ has not directed to any symmetric axis of the lattice, the energy splitting leads to the complete degeneracy removal except for the spin degeneracy. Conformably, the ground-state energy splits into the six different levels as is seen in Fig. 3.

What energy level of the six ones written in the Eq. 9 is the lowest? It depends on the relationship between h_x, h_y, and h_z which define the off-diagonal s−p type matrix elements $V_a(\mathbf{h})$. For example, in case $h_x > h_y > h_z > 0$ (this is the case shown in Fig. 3) the energy $E_z^{(-)}$ becomes the lowest. Evidently, there are six different groups of relationships between the components h_a (each group contains eight relationships), every one of which defines new ground state from the set (13). Each of the 48 relationships describes the spherical sector in space of the impurity position-vector within the quantum dot. In a certain sense one may say that belonging of the vector $\mathbf{h}$ to one of these sectors fixes one of the states (13) to be the ground.

As is seen in the figure, the splitting of each the twofold level E_{0e}, corresponding to a certain X-point, is sufficiently great except for the cases when the donor is situated near the dot center or the interface. For intermediate values of the ratio h/R, the splitting caused by the system asymmetry achieves several tens (or, even, hundred) of meV. At least for lithium, this is expected to be considerably greater than the valley–orbit splitting. As has been shown earlier [10, 11] the valley–orbit splitting in quantum dots sharply decreases if $h \to R$, and equals zero at the dot boundary. At the same time, at $h \to 0$, it has some nonzero value. Therefore, the curves presented in Fig. 3 should be slightly corrected at small h/R. However, such a correction does not exceed, apparently, several meV for 3 nm nanocrystal doped with Li, and may be neglected.

Let us now discuss the modification of the ground electron state due to the hidrogen-like donor. Because of the donor existence inside the dot, the ground-state wave function $\Psi_z^{(-)}$ acquires some first-order correction that can be represented as the product of two factors. The first one is the correction to the envelope-function

$$\begin{aligned}\Delta F_z^{(-)} = {} & -\frac{V_z(\mathbf{h})\sec\lambda}{E_{2e} - E_{0e}}|p_z\rangle\\ & - \frac{\cos\lambda}{E_{1e} - E_{0e}} \frac{V_x(\mathbf{h}) + V_y(\mathbf{h})}{\sqrt{2}} \frac{|p_x\rangle + |p_y\rangle}{\sqrt{2}},\end{aligned} \tag{14}$$

while the second factor is the Bloch function $(|Z\rangle - |Z'\rangle)/\sqrt{2}$ of the irreducible representation $\Delta_{2'}$. It is convenient to introduce the unit vector $\mathbf{n} = \mathbf{h}/h$ along the

donor's position-vector. Then the donor site can be defined with n_x, n_y, n_z, and h. To illustrate the role of donors in a reconstruction of the electron wave function and, as a consequence, in a redistribution of the electron density, we choose $n_x = 0.8$, $n_y = 0.5$, $n_z = 0.33$ and plot the envelope-function correction $\Delta F_z^{(-)}$ as a function of the electron position (i) at the radial axis $\mathbf{r} \parallel \mathbf{h}$, and (ii) on the sphere $r = h$, see Figs. 4 and 5, respectively.

Figure 4 represents the dependence of $\Delta F_z^{(-)}$ (dashed and dotted lines) on the electron position at the axis drawn through the donor and the dot center. In this case electron position-vector $\mathbf{r}$ is strictly parallel or antiparallel to $\mathbf{h}$. For comparison, the zeroth-order envelope function of s-type has been also plotted in the figure with solid line.

Since we direct the radial axis parallel to $\mathbf{h}$, the donor is always situated somewhere at the right half of this axis within the range $0 < h/R < 1$. We have calculated $\Delta F_z^{(-)}$ for three different positions of the donor ion inside the dot. When the donor is close to the dot center ($h/R = 0.1$), the first-order correction is small enough, as was already pointed out earlier. At $h/R = 0.46$, the correction becomes the greatest. Further increase of h/R leads to the general reduce of $\Delta F_z^{(-)}$. Such the behavior of $\Delta F_z^{(-)}$ has the simple explanation. The first-order correction $\Delta F_z^{(-)}$ is directly proportional to the off-diagonal Coulomb matrix elements of s−p type, see Eq. 14. Meanwhile, these matrix elements rise from zero at $h = 0$ to their maximum taking place exactly at $h/R = 0.46$. Then, V_a decreases as h increases, as it is shown in Fig. 1. Thus, the correction $\Delta F_z^{(-)}$ qualitatively follows, in fact, the dependence V_a on h.

It is also seen in Fig. 4 that the maximum of all three curves takes place approximately at $r/R = 0.46$ and does not depend on h. The latter is a consequence of the "two-level" approximation accepted in Eq. 7. If we take into account not only the lowest s- and p-states, the dependence of the first-order correction $\Delta F_z^{(-)}$ on h appears at once. Nevertheless, such the rough approximation turns out to be quite correct and sufficient to describe the general trend in behavior of $\Delta F_z^{(-)}$ as a function of r. In particular, $\Delta F_z^{(-)}$ is always positive when $\mathbf{r} \parallel \mathbf{h}$, i.e., the donor and electron are situated at the same half of the axis. This means that the probability to find the electron near the donor site rises, while on the other side relative to the dot center the probability reduces. Thus, the electron-density distribution becomes asymmetric. It rises along the vector $\mathbf{h}$, and reduces along the opposite direction.

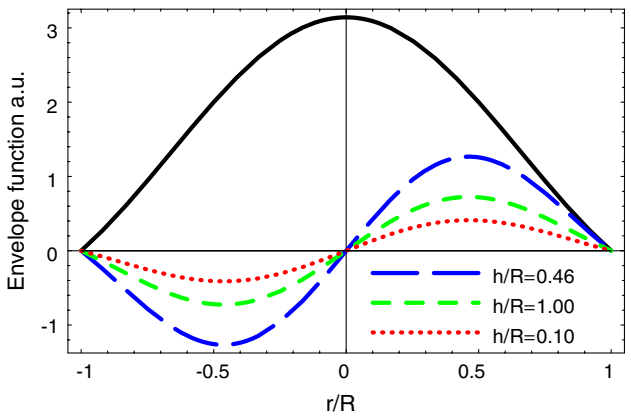

Fig. 4 The first-order corrections (dashed and dotted lines) to the envelope function of the s-type (solid line) in arbitrary units. $n_x = 0.8$, $n_y = 0.5$, $n_z = 0.33$. $\mathbf{e} = \mathbf{n}$. $R = 1.5$ nm

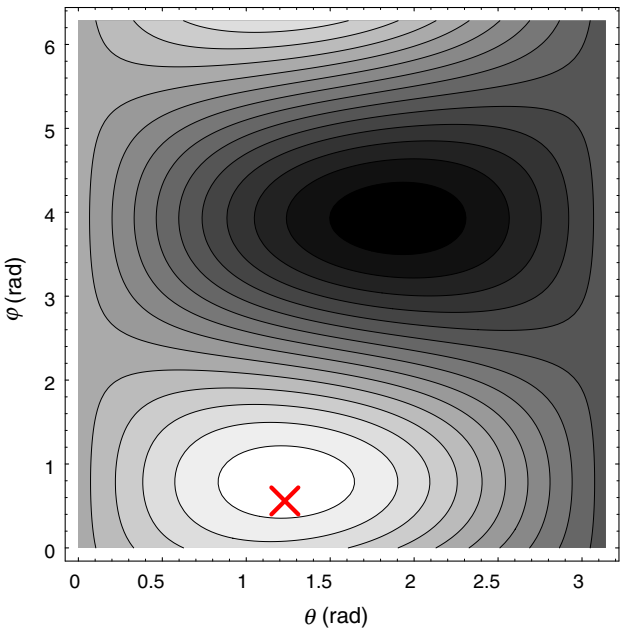

Fig. 5 Contour plot of the first-order correction $\Delta F_z^{(-)}$ at $n_x = 0.8$, $n_y = 0.5$, $n_z = 0.33$ for 3 nm quantum dot. The value of $\Delta F_z^{(-)}$ rises from dark to light. The cross indicates the donor position

We have also plotted in Fig. 5 $\Delta F_z^{(-)}$ as a function of the angles θ and φ on the spherical surface $r = h$ for the former values of n_a. The angles θ and φ are introduced in the standard form: $e_x = \sin\theta\cos\varphi$, $e_y = \sin\theta\sin\varphi$, and $e_z = \cos\theta$, where e_a is an a-component of the unit vector $\mathbf{e} = \mathbf{r}/r$. Because the envelope functions $|p_a\rangle$ and Coulomb matrix elements $V_a(\mathbf{h})$ are directly proportional to e_a and n_a, respectively, the angle dependence of $\Delta F_z^{(-)}$should be sensitive to the donor position on the sphere. This is completely confirmed by our calculations presented in the figure. As is seen, maximal values of $\Delta F_z^{(-)}$ (light areas in the figure) are located around the donor site marked with the cross. However, it is also seen that the cross does not fully coincide with the center of the brightest spot. The nature of this discrepancy, apparently, may be explained by the use of the "two-level" approximation as well.

Conclusion

Let us now briefly describe the obtained results. First, we have found analytical expressions for the electron energies and wave functions in case of arbitrary donor position inside the quantum dot. Note for comparison that more general treatment [10, 11], taking into account dominant role of the central-cell potential, permits of only numerical calculations. Second, it has been shown that, the wave functions in Li-doped nanocrystals have already no the symmetry of tetrahedral group T_d, or close to that, as it took place for V-group donors in the bulk, or nanocrystals, respectively, even in the case of asymmetric donor position inside the nanocrystal [10, 11]. This is due to disappearance of the short-range Coulomb field that symmetrizes the Bloch functions according to the symmetry transformations of the point group T_d. Third, energy splitting for a hydrogenlike lithium donor essentially differs from that for V-group donors creating the central-cell field. Provided that the valley–orbit interaction is taken into account, the splitting occurs even for the case of central located donor inside the dot. On the contrary, if we deal with the lithium donor, the splitting is absent in case $h = 0$ as is seen in Fig. 3. At last, fourth, the presence of a donor inside the nanocrystal leads to the substantial relocation of the electron density (up to 10%, see Fig. 4) towards the donor. This, in turn, leads to the reconstruction of the electron wave functions and subsequent polarization of the electron subsystem in the dot. Such the polarization, undoubtedly, should influence the values of electron–photon matrix elements and the transition probabilities on the whole.

Acknowledgments The authors thank the Russian Ministry of Education and Science, and the Russian Foundation for Basic Research for the financial support of this work through the program "Development of a scientific potential of the high school" (the project No 2.1.1.2363), and the project No 05-02-16762, respectively.

References

1. M. Fujii, A. Mimura, S. Hayashi, K. Yamamoto, Appl. Phys. Lett. **75**, 184 (1999)
2. A. Mimura, M. Fujii, S. Hayashi, D. Kovalev, F. Koch, Phys. Rev. B **62**, 12625 (2000)
3. M. Fujii, Y. Yamaguchi, Y. Takase, K. Ninomiya, S. Hayashi, Appl. Phys. Lett. **85**, 1158 (2004)
4. D.I. Tetelbaum, S.A. Trushin, V.A. Burdov, A.I. Golovanov, D.G. Revin, D.M. Gaponova, Nucl. Instr. Meth. B **174**, 123 (2001)
5. G.A. Kachurin, S.G. Cherkova, V.A. Volodin, V.G. Kesler, A.K. Gunakovsky, A.G. Cherkov, A.V. Bublikov, D.I. Tetelbaum, Nucl. Instr. Meth. B **222**, 497 (2004)
6. Y. Hada, M. Eto, Phys. Rev. B **68**, 155322 (2003)
7. D.V. Melnikov, J.R. Chelikowsky, Phys. Rev. Lett. **92**, 046802 (2004)
8. Z. Zhou, M.L. Steigerwald, R.A. Friesner, L. Brus, M.S. Hybertsen, Phys. Rev. B **71**, 245308 (2005)
9. Q. Xu, J.-W. Luo, S.-S. Li, J.-B. Xia, J. Li, S.-H. Wei, Phys. Rev. B **75**, 235304 (2007)
10. V.A. Belyakov, V.A. Burdov, Phys. Rev. B **76**, 045335 (2007)
11. V.A. Belyakov, V.A. Burdov, Phys. Lett. A **367**, 128 (2007)
12. R. Tsu, D. Babic, Appl. Phys. Lett. **64**, 1806 (1994)
13. M. Lannoo, C. Delerue, G. Allan, Phys. Rev. Lett. **74**, 3415 (1995)
14. R. Tsu, D. Babic, L. Ioriatti, J. Appl. Phys. **82**, 1327 (1997)
15. S. Ogut, R. Burdick, Y. Saad, J.R. Chelikowsky, Phys. Rev. Lett. **90**, 127401 (2003)
16. C. Delerue, M. Lannoo, G. Allan, Phys. Rev. B **68**, 115411
17. X. Cartoixa, L.-W. Wang, Phys. Rev. Lett. **94**, 236804 (2005)
18. F. Trani, D. Ninno, G. Cantele, G. Iadonisi, K. Hameeuw, E. Degoli, S. Ossicini, Phys. Rev. B **73**, 245430 (2006)
19. S.T. Pantelides, C.T. Sah, Phys. Rev. B **10**, 621 (1974)
20. F. Bassani, G. Iadonisi, B. Preziosi, Rep. Prog. Phys. **37**, 1099 (1974)
21. S.T. Pantelides, Rev. Mod. Phys. **50**, 797 (1978)
22. W. Kohn, J.M. Luttinger, Phys. Rev. **97**, 1721 (1955)
23. W. Kohn, J.M. Luttinger, Phys. Rev. **98**, 915 (1955)
24. R.A. Faulkner, Phys. Rev. **184**, 713 (1969)
25. C. Delerue, M. Lannoo, *Nanostructures. Theory and Modelling*, Springer-Verlag Berlin Heidelberg (2004)
26. V.A. Burdov, Zh. Eksp. Teor. Fiz. **121**, 480 (2002) [JETP **94**, 411 (2002)]
27. D.H. Feng, Z.Z. Xu, T.Q. Jia, X.X. Li, S.Q. Gong, Phys. Rev. B **68**, 035334 (2003)
28. A.S. Moskalenko, I.N. Yassievich, Fiz. Tverd. Tela (St. Petersburg) **46**, 1465 (2004); Phys. Solid State **46**, 1508 (2004)
29. A.A. Kopylov, Fiz. Tekh. Poluprovodn. (Leningrad) **16**, 2141 (1982); Sov. Phys. Semicond. **16**, 1380 (1982)